Nuclear Engineering and Design 429 (2024) 113621

Contents lists available at ScienceDirect

Nuclear Engineering and Design

journal homepage: www.elsevier.com/locate/nucengdes

Pre-disposal management of spent ion-exchange resins by Fenton oxidation treatment and conditioning in an alkali-activated matrix

Francesco Galluccio [a], Andrea Santi [a], Eros Mossini [a,*], Gabriele Magugliani [a], Fabio Fattori [a], Giacomo Diego Gatta [b], Paolo Lotti [b], Davide Cori [c], Elena Macerata [a], Gianmarco Bilancia [d], Mario Mariani [a]

[a] Department of Energy, Politecnico di Milano, Piazza Leonardo da Vinci 32, 20133 Milano, Italy
[b] Department of Earth Sciences, University of Milan, Via Sandro Botticelli 23, 20133, Milano, Italy
[c] Nucleco S.p.A., Via Anguillarese 301, 00123, Roma, Italy
[d] Joint Research Centre, European Commission, Via Enrico Fermi 2749, 21027 Ispra, Italy

ARTICLE INFO

Keywords:
Nuclear waste management
Spent ion-exchange resins
Fenton wet oxidation
Alkali-activated matrix

ABSTRACT

The routine use of ion-exchange resins throughout the lifecycle of a nuclear facility poses significant issues regarding their safe and sustainable disposal at the end of their useful life. Effective strategies are thus required to overcome the challenging nature of this organic waste, aimed at minimizing volumes of the final waste forms, processing costs, and environmental impact. This work focuses on the pre-disposal management of spent mixed bed resins through the integration of a Fenton oxidative treatment process, an attractive environmentally friendly approach, and the successive encapsulation of the residues in an alkali-activated matrix. The successful treatment of a 20 g mix of cationic and anionic resins has led to a preliminary upscale of the process by using a surrogate waste (up to 200 g) loaded with representative activation and fission products contaminants. Some important process parameters were monitored, and the resulting residues were characterized. Finally, the obtained residues were encapsulated in an alkali-activated matrix with a loading factor up to 40 wt.%. Waste forms with residue loading factors up to 10 wt.% (corresponding to the conditioning of 0.6 kg of spent resin per kg of matrix) achieved preliminary compliance with waste acceptance criteria.

1. Introduction

Over the years, the use of ion-exchange resin (IER) has become paramount for the chemical control of water and the removal of radioactivity during nuclear power plant operations, as well as for the decontamination of different liquid waste streams during decommissioning stages of a nuclear facility. Moreover, other nuclear industrial applications are employing cationic, anionic, and mixed bed ion exchange resin systems (International Atomic Energy Agency, 2017). Besides the progressive saturation of the ion-exchange sites, the harsh conditions of use, namely high temperatures and radiation fields, adversely impact on the performance of IERs, thereby reducing their permeability, selectivity, and affinity towards contaminants. Even though IERs could be partially regenerated and reused, they are usually replaced to reduce the amount of radioactive liquid waste generated (Castro et al., 2018). This approach leads to the worldwide production of large volumes of exhausted organic resins, as between 10 and 50 m^3, depending on the type of nuclear power reactor, are yearly generated (International Atomic Energy Agency, 1993; Office of Federal et al., 2013). What is more, some European countries have to manage large amounts of IERs which pose issues about their radiological characterization, because they were conditioned several years ago.

Spent IERs are generally classified as low- or intermediate-level waste (Wang et al., 2015). In order to ensure the sustainability of nuclear power production, a suitable waste route should be developed to safely dispose of spent IERs in national repositories. Their direct encapsulation in Portland cement or bitumen was widely pursued in the past, with the intent of obtaining solid and stable waste forms, thus reducing potential migration of radionuclides towards the biosphere (International Atomic Energy Agency, 2001). However, the scarce loading capacity (about 10 wt.%) generates large volumes of final waste forms, which result in high costs and relevant environmental footprint. Moreover, the poor stability of the waste packages because of the swelling of the beads, and the challenging nature of the waste, related to potential flammability, leachability of radionuclides, and microbial activity hinder the compliance with the waste acceptance

* Corresponding author.
E-mail address: eros.mossini@polimi.it (E. Mossini).

https://doi.org/10.1016/j.nucengdes.2024.113621
Received 7 August 2024; Received in revised form 30 September 2024; Accepted 1 October 2024
Available online 10 October 2024

criteria (WAC) demanded by modern nuclear waste repositories (International Atomic Energy Agency, 2017). This led to the development of more reliable conditioning matrices and treatment processes to destroy the organic component (Pan et al., 2009). Such a task was also the main scope of the Work Package 6 (*Innovation in solid organic waste treatment and conditioning*) within the EU-H2020 PREDIS (*PRE-DISposal management of radioactive waste*) project, a collaborative network of several European partners supported by a strong end-user group, in which this research work was performed (Oksa et al., 2021).

Some advanced oxidative treatments such as dry and wet oxidations appear as promising solutions in managing spent organic resins (Wang et al., 2015). Nevertheless, some critical issues, such as incomplete burning, off-gas treatment and monitoring, and potential radionuclide volatilization because of high operating temperatures, are hindering the full implementation of dry treatments like incineration, while incomplete organic decomposition could hold back the development of wet oxidation. A Fenton wet oxidative process can be considered more attractive thanks to lower operating temperatures, and the use of cheap and green reagents (Wang et al., 2015). Once the oxidative reaction is triggered, the self-sustaining process can be operated at temperatures close to 100 °C, thereby minimizing the energetic cost and the issue of off-gas treatment, but also reducing the risk of corrosion from organic acids and the potential volatilization of radionuclides (Walling et al., 2021). Eventually, the obtained final residue should be characterized and immobilized into a stable matrix to allow its safe disposal. The acidity (pH around 1–2) and the high content of sulphates of such residues usually hinder their encapsulation with a high LF in common cement-based matrices (Taylor et al., 2001).

Despite its scarce mainstream success for a full commercial implementation, the Fenton wet oxidation has always drawn great attention from the research community to successfully treat a wide variety of problematic organic waste, from wastewaters to spent IERs (Walling et al., 2021). Advancements in the original Fenton process have been achieved by using alternative homogeneous catalysts other than Fe such as Cu, sometimes used in multi-element catalyst systems (Bokare et al., 2014). Moreover, some advanced setups equipped with an external source of energy such as the photo-, electro-, and sono-Fenton are being used separately or in combined configurations to enhance the oxidation yield of some problematic organic wastes despite the increased complexity and energy consumption (Lama et al., 2022; Wang et al., 2016). Several research works have already investigated the feasibility and optimization of the homogeneous oxidative treatment of small batches of mainly cationic resin, while very few others focus on the management of a mixed resin bed (Meng et al., 2022; Feng et al., 2018; De Araujo et al., 2018). Most of the literature studies mainly shed light on the optimization of the complex operational set of reaction parameters that strongly affect the success of the oxidative treatment. A lot of effort was put on exploring the effects of the initial temperature, type and dosage of catalysts, amount of oxidant (H_2O_2), and pH value (Zahorodna et al., 2007; Hafeez et al., 2021). The best operational conditions are generally identified, based on the highest organic matter decomposition measured by COD or total organic carbon (Xu et al., 2019; Wan et al., 2015). For instance, an excess of oxidant or catalyst, low initial temperature and pH beyond a limited range do not promote the formation of the strongly reactive OH· radicals able to decompose organic matter, but trigger instead competitive reactions which increase the production of secondary waste and the costs of the treatment (Huang et al., 2020).

On the other side, alkali-activated matrices are showing as promising candidates. Such materials consists of amorphous binders which are obtained by alkaline activation of aluminosilicate precursors at room temperature (Autef et al., 2013; Görhan et al., 2014; Lee et al., 2019). A wide range of wastes with different physico-chemical properties may be proficiently encapsulated in these matrices (de Oliveira et al., 2022; Ahmed et al., 2021; de Azevedo et al., 2017). In particular, compared to cements, these materials are usually endowed with better compatibility with wastes containing residual organic matter and elevated salinity, such as wet oxidation residues, thus ensuring higher waste LF and limiting the increase of final volume (Reeb et al., 2021; Khalifeh et al., 2014). In addition, such matrices have shown better chemical and thermal durability properties, making them more suitable for radioactive waste confinement (Singh et al., 2015). Additionally, alkali-activated matrices are more sustainable than cements since the precursors can consist of recycled industrial by-products, thus pursuing the goals of environmental sustainability and circular economy, and of natural materials, such as volcanic tuffs rich in zeolites. Zeolitic tuffs are worldwide-available, low-cost, untreated materials, capable of providing remarkable waste-matrix interactions via ion-exchange processes (Cappelletti et al., 2011; Baek et al., 2018), thus promisingly reducing the leachability of some contaminants (Dyer et al., 2000). Indeed, zeolites have been widely considered as additives to cemented forms to reduce the release of contaminants and increase the overall stability (Dyer et al., 2000; Rozek et al., 2019; Junfeng et al., 2005).

The optimal operating conditions of the Fenton oxidation treatment employed in this work, namely the start-up temperature, the amount of both catalyst and oxidant, and the process duration, were derived from those already identified in other research works (Meng et al., 2022; Xu et al., 2019; Galluccio et al., 2021). Hence, efforts have been aimed at demonstrating the applicability to real waste management scenarios which entail the integration between treatment and conditioning steps to allow the disposal of spent IERs. A surrogate waste was prepared by loading the mixed bed resin with representative activation and fission products contaminants to mimic the composition of real spent IERs, serving as a relevant case for the nuclear industry end-users. The characterization of the obtained effluents and the distribution of representative contaminants have been investigated. The adopted oxidative conditions, based on literature evidence, consist of an exothermic reaction of an oxidant (H_2O_2) with a co-catalyst system (aqueous $FeSO_4$ and $CuSO_4$) to promote the formation of strongly reactive radicals HO·, which in turn trigger the dissolution and mineralization of the organic matter into small molecular organic species (Zahorodna et al., 2007). Moreover, although the regeneration of primary catalyst Fe^{2+} and Cu^{+} ions is very slow, the overall oxidative process is self-sustaining, albeit for a limited time (Walling et al., 2021; Bokare et al., 2014).

After the treatment, the efforts have been focused on the conditioning of the obtained residues to produce a stable and durable waste form suitable for disposal. The accomplishment of this step is imperative for the successful development of an integrated waste management strategy. For the first time, according to authors' knowledge, the wet oxidation residues obtained downstream of the evaporation stage were mixed in a fresh non-cementitious paste. A tuff-based alkali-activated matrix (Santi et al., 2022), recently developed, has been considered and tested in this work. The tested encapsulation strategy consisted in introducing increasing amounts of wet oxidation residues, duly neutralized with sodium hydroxide, into the matrix fresh grouts, with LF up to 40 wt.% (equivalent to 3.3 kg of spent resins per kg of binding matrix). Overall, a complete pre-disposal solution is proposed in this work, to manage a surrogate mixed bed resin loaded with contaminants as a more representative case of the nuclear industry.

2. Material and methods

2.1. Chemicals and materials

The IERs used in this work are nuclear-grade, strong cationic and anionic, styrene–divinylbenzene co-polymers AmberLite™ IRN 77 and IRN 78, commercialized by DuPont™. The main features of these resins are reported in data sheets of the products (DuPont, 2023a,b). Cationic resins were loaded with Co^{2+} , Ni^{2+} , Sr^{2+} , and Cs^{+} ions. A stock solution was prepared by dissolving weighed amounts of the nitrate salts of the above-mentioned elements (Sigma-Aldrich, analytical grade) in 1.0

Table 1
Chemical composition of the main matrix precursors used in the alkali-activated matrix, expressed in wt.%.

Material	Al_2O_3	CaO	Fe_2O_3	K_2O	MgO	MnO	SiO_2	H_2O
VT	17.8 ± 0.3	8.3 ± 0.3	5.7 ± 0.2	7.0 ± 0.1	1.3 ± 0.1	0.2 ± 0.1	57.3 ± 0.5	0.9 ± 0.1
FA	21.3 ± 0.1	3.9 ± 0.1	8.1 ± 0.1	3.3 ± 0.1	1.4 ± 0.1	0.1 ± 0.1	59.0 ± 0.2	0.1 ± 0.1
BFS	5.9 ± 0.1	40.3 ± 0.1	0.7 ± 0.1	0.5 ± 0.1	3.6 ± 0.1	0.1 ± 0.1	26.1 ± 0.1	0.1 ± 0.1

M HNO_3 to obtain a 0.2 M final concentration of each metal. Similarly, another stock solution was prepared by dissolving KI and KCl salts in de-ionized water to a 0.2 M final concentration to load anionic resin batches.

The chemicals used for the wet oxidative process consist of $FeSO_4 \cdot 7\ H_2O$ and $CuSO_4 \cdot 5\ H_2O$ catalysts (analytical-grade reagent supplied by Sigma-Aldrich), and H_2O_2 oxidant (35 wt.% technical-grade reagent provided by Chimitex S.p.A., Italy). Catalyst solutions of 0.1 M were prepared by dissolving salts in deionized water.

The matrix precursors, used without further processing, were micronized volcanic tuff (VT) (Zeolite Fertenia™), class F fly ash (FA) and ground-granulated blast-furnace slag (BFS) provided by Buzzi Unicem, Italy. The compositions of these materials are reported in Table 1: in triplicate, oxides were determined by means of X-ray fluorescence (XRF), while water content was assessed via thermogravimetry. Aluminium oxide (MERCK, analytical grade), for Si/Al stoichiometric balance (Firdous et al., 2018), and sodium hydroxide (Sigma-Aldrich, analytical grade), for alkali activation, were added as well. The main properties of these materials are described elsewhere (Santi et al., 2022).

2.2. Loading of the mixed bed resin

The solutions for cationic and anionic resins loading were prepared from the respective stock solutions by dilution with nitric acid or deionized water. Suitable amounts of cationic and anionic resin (10 g, 50 g, 100 g) were weighed in 1:1 mass ratio, placed in beakers, and separately contacted with the corresponding loading solution under vigorous mixing for about 2 h. Afterwards, the solutions were separated by decanting, and the loaded resins, duly washed with de-ionized water, were air-dried to constant mass overnight to remove excess water. Aliquots of the solutions were taken before and after the contacting stage to evaluate the LF via inductively coupled plasma mass spectrometry (ICP-MS) analysis. The saturation factor with respect to the ion exchangeable sites of the mixed bed ranged from 10 eq.% to 40 eq.%.

2.3. Wet oxidation setup

The following experimental setup, shown in Fig. 1, was arranged:

- four-necked round-bottom flask as glass reactor (500 mL and 3000 mL) used for small (20 g) and intermediate (100 and 200 g) laboratory scale processes, respectively;
- stirring heating mantle or hot plate with thermal bath to control the start-up temperature and ensure proper mixing throughout the process;
- glass thermometers to monitor the process temperature of the wet oxidation solution and thermal bath over time;
- peristaltic pump to ensure constant flow rate addition of the oxidant into the glass reactor containing the resin and the catalyst;
- condenser and receiving flask to condense released vapours;
- bubblers filled with proper solutions (*e.g.*: NaOH and H_2SO_4) may be used downstream of the glass reactor to trap CO_2 and other volatile species (*e.g.*: iodine and chlorine).

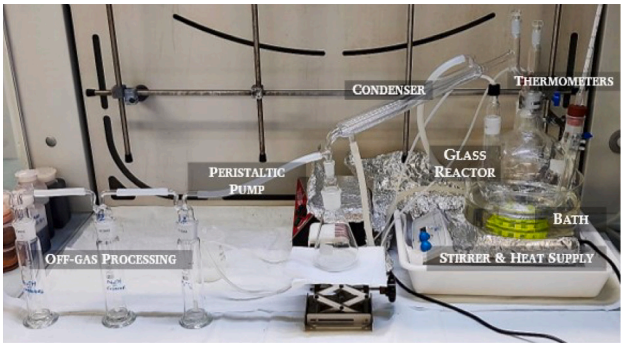

Fig. 1. Experimental setup used for the laboratory oxidative process.

Table 2
Process parameters of wet oxidative treatments at small and intermediate laboratory scale. The catalyst solution is deionized water containing 0.1 M Fe^{2+} and 0.1 M Cu^{2+}.

Resin bed mass (g)	Catalyst solution (mL)	Oxidant flow rate (mL min^{-1})	Oxidant (mL)	Reaction time (h)
20	100	1	180	3
100	500	1 → 2	960	8
200	500	1 → 2	1720	15

2.4. Fenton oxidation process

The simulant waste and the catalyst solutions were added to the glass reactor, and the pH, initially adjusted to around 2 with sulphuric acid, was carefully monitored over time throughout the process to guarantee, according to the literature, the highest resin degradation rate by enhancing the formation of reactive HO· species and discouraging all the scavenging competitive reactions (Hafeez et al., 2021; Xu et al., 2019; Liou et al., 2005; Vilve et al., 2010; Zahorodna et al., 2008). Once the start-up temperature of the process was achieved (at least 45 °C), the oxidant was added at controlled flow rate by means of a peristaltic pump to safely trigger the oxidation process, as reported in Table 2. The optimal start-up temperature, catalyst and oxidant amount, and process duration were retrieved from previous experimental findings on merely cationic resin treatment (Galluccio et al., 2021). As a matter of fact, the process has not a linear response (Table 2), and the presence of anionic resin in this case made it more challenging. During the process, after the gross decomposition of the cationic resin beds, the oxidant flow rate was also doubled to facilitate the longer-lasting decomposition of the anionic resin. To follow the process, temperature and colour of the mixture were monitored over time. Besides, aliquots of the wet oxidation solution were periodically collected to be characterized. At the end of the process, the mixture was collected from the reactor and weighed. A clear solution was obtained by filtration and a whitish precipitate was retrieved if further characterization was needed. Otherwise, the mixture comprising the clear solution and the precipitate went to the next step.

2.5. Conditioning of the residues

The mixture resulting from wet oxidation treatments was transferred in a beaker and weighed. Thereafter, it underwent evaporation at controlled temperature (about 70 °C) in order to discourage potential

Table 3
Composition of the raw materials for the preparation of the waste forms.

Composition (wt.%)						
Waste residue	Tuff	Fly ash	Slag	Alumina	Hydroxide	Water
0.0	14.7	24.1	24.1	2.0	8.1	27.0
10.0	13.0	21.3	21.3	1.8	8.7	23.9
20.0	11.3	18.6	18.6	1.5	9.2	20.8
28.0	10.0	16.3	16.3	1.4	9.7	18.3
34.0	9.0	14.7	14.7	1.2	10.0	16.4
40.0	7.9	13.0	13.0	1.1	10.4	14.6

leakage of volatile nuclides. The process took up to 24 h, depending on the initial mass of the surrogate waste. After the removal of the free water, the obtained brownish residues were weighed and the weight reduction ratio (WRR) was computed according to the following equation:

$$\mathrm{WRR} = 1 - \frac{m_{\mathrm{w}}}{m_{\mathrm{res}}}, \tag{1}$$

where m_{res} is the initial mass of resin after loading the contaminants and m_{w} is the mass of the final residue after the evaporation process. Eventually, the residue was conditioned in the matrix. The fresh grout was prepared, and the residue was mixed in it, then the paste was cast and left to set prior to further testing.

The conditioning matrix proposed to immobilize the residues downstream of the treatment process is an alkali-activated formulation derived from the results obtained in a previous study (Santi et al., 2022). The amounts for the recipes are reported in Table 3. Because of the very low pH of the residues obtained downstream of the Fenton treatment, a basification step (until pH close to 9) prior to conditioning is required since the acidity would consume the NaOH needed for the alkali-activation of the conditioning matrix precursors. The matrix was prepared by weighing the solid powders, namely VT, FA, BFS, and alumina, and homogenizing them in a planetary mixer at low speed. The sodium hydroxide and the water were then added. Mixing was carried out for ten minutes at low speed, then the residue from wet oxidation was added and the grout was mixed for other ten minutes. The LF of the waste form is computed as follows:

$$\mathrm{LF} = \frac{m_{\mathrm{r}}}{m_{\mathrm{g}}}, \tag{2}$$

where m_{r} and m_{g} are, respectively, the masses of the Fenton treatment residue and that of the resulting fresh grout. The mass m_{g} in Eq. (2) accounts for the extra sodium hydroxide needed for the neutralization of the Fenton residue. Fresh grouts were cast afterwards in different moulds, depending on the specific purpose as described in the next section, and were left to cure in endogenous conditions for 28 days prior to testing.

2.6. Assessment of durability

A stepwise approach was followed to preliminarily assess the regulatory compliance of the management strategy proposed in this work. A screening among the LFs was performed taking into account hardening and the resistance towards static immersion in water. A deeper assessment of the durability was performed in agreement with the Italian WAC by means of compression and leaching tests (Ispettorato nazionale per la sicurezza nucleare e la radioprotezione, 2022).

Firstly, 3-cm equilateral cylindrical specimens were cast at different LFs, ranging from 0 to 40 wt.%. Such specimens were prepared to screen the various formulations according to hardening of the waste forms and their stability towards static immersion in deionized water for two weeks. After testing, the immersed specimens were left to dry in air prior to visual inspection. Formulations which did not harden at 28 days of curing, or which exhibited cracking following the static immersion were discarded.

Following the screening step, a more robust characterization involving the measurement of compressive strength and the resistance towards leaching was performed. Compressive strength was measured on cubic samples with sides of 5 cm. The tests were carried out according to EN 12390-3:2019 standard protocol (European Committee for Standardization, 2019). The reference compressive strength for conditioned waste forms at Italian level is 10 MPa at 28 days (Ispettorato nazionale per la sicurezza nucleare e la radioprotezione, 2022). This value was set as the reference for this work because it is more restrictive than the requirements imposed by the regulatory authorities of other countries. Leaching tests were carried out in ultrapure water on 3-cm equilateral cylindrical specimens according to the ANSI/ANS-16.1-2019 protocol (American National Standards Institute, 2019). Aliquots of the leachates were taken, acidified with ultrapure nitric acid, and duly diluted for inductively coupled plasma optical emission spectroscopy (ICP-OES) and ICP-MS analyses.

2.7. Instrumentation

The COD of aliquots periodically collected during the wet oxidation process was measured, after proper dilution, by COD Cell Tests kit (Spectroquant, 25–1500 mg L^{-1}, Supelco-Sigma-Aldrich) (Desotelle, 1999; International Standardisation Organisation, 2022). Because of resin insolubility in water, first reference measurements can be considered 20 min after the beginning of the treatment.

Element concentrations to monitor the distribution of nuclides throughout all process stages (resin loading, wet oxidation process, and analysis of leachates) were determined with a Avio™ 500 ICP-OES spectrometer (Perkin Elmer) and a NexION™ 2000 ICP-MS spectrometer (Perkin Elmer). The calibration of the instruments was performed by using Inorganic Ventures CMS-x standard solutions diluted at different concentrations, depending on the investigated elements and range of concentrations.

X-ray powder diffraction (XRD) analysis was conducted with an automated Panalytical X'Pert Pro modular diffractometer, equipped with a X'Celerator detector, according to the following operating conditions: monochromatized Cu-Kα radiation, 40 kV, 40 mA, 2θ range from 4 to 80° and step size of 0.017°, counting time of 240 s per step. All the diffraction peaks were indexed and assigned, using the database of the crystalline species of the X'Pert HighScore suite, providing an unambiguous scenario about the crystalline phase identification. Obtained patterns were plotted with Origin software in the 2θ range from 5° to 65°.

Cubic specimens underwent uni-axial compression following the EN 12390-1:2019 (European Committee for Standardization, 2021) and EN 12390-3:2019 (European Committee for Standardization, 2019) standards, applying a loading rate within the range 0.6 ± 0.2 MPa s^{-1}. The compressive strength was derived as the ratio of the maximum applied load and the cross section of the specimen and expressed in MPa.

The porosity of the waste forms was assessed with a Autopore IV 9500 mercury intrusion porosimeter by Micromeritics using a protocol derived from literature (Perez-Cortes et al., 2024). Fragments of samples (approximately 0.500 g) cured at 28 days were left to dry under vacuum for 24 h at room temperature. After retrieval, the specimens were inserted in the porosimeter bulb and pressure was applied in the range 1–200 MPa. The distribution of the pore sizes was derived according to the Washburn equation (Gallé, 2001) assuming a sample-mercury contact angle of 130°.

3. Results and discussion

3.1. Fenton oxidation treatment

3.1.1. Proof of concept (20 g)

The decomposition of a mixed bed resin was firstly demonstrated by treating about 20 g of unloaded mixed resin beads. In accordance with

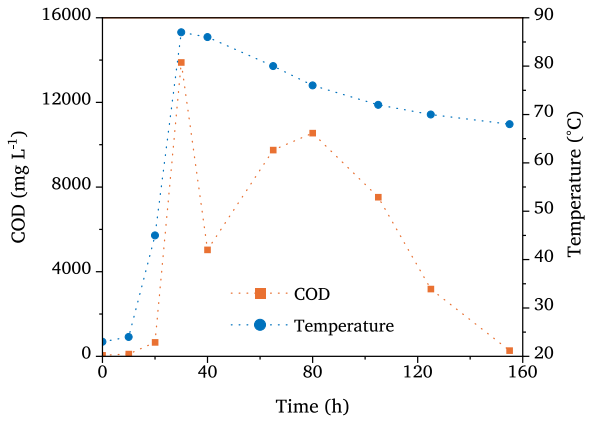

Fig. 2. Reaction temperature and COD profiles as a function of time measured throughout the oxidative process. The uncertainty related to temperature values is ± 1 °C, while a range of ± 5% can be considered for COD measurements.

literature and based on preliminary experimental findings, the presence of anionic resin required the addition of $CuSO_4$ to be synergically employed with $FeSO_4$ as co-catalyst system to boost the oxidation yield of the surrogate waste (Wan et al., 2016). The monitoring of reaction temperature showed a peak of about 90 °C at early stage without any external heat supply, as depicted in Fig. 2. After 1 h, a second broad reaction peak at about 80 °C was observed. Thereafter, the temperature decreased until the end of oxidation and mineralization of mixed resin beads. Besides temperature, the colour shift of the mixture was helpful to monitor the evolution of the treatment process (Fig. 3). Indeed, the orange resin mixture gradually turned dark in correspondence with the first temperature peak, then hazel-coloured and eventually light yellow, as the organic matter completely degraded within about 3 h. In addition, a whitish and fine residue without any resin beads was found at the bottom of the reactor.

The effective IERs mineralization was proved by measuring the COD of the aliquots collected as a function of time throughout the wet oxidation process. As shown in Fig. 2, a double-peak reaction was found. A steep increase of COD can be observed at early stages, in correspondence with the first temperature peak, when the cationic IER dissolution occurs. Thereafter, smaller values due to progressive resin decomposition and a second broader peak can be observed in accordance with the temperature profile and colour of the solution. This second peak may be ascribed to the subsequent degradation of the anionic IER. At the end of the process, the COD returned close to the initial value measured on the mixture before the occurrence of the IER degradation. This means that the dissolved organic matter has been greatly degraded.

3.1.2. Laboratory upscale (100 g and 200 g)

After verifying the successful treatment of a 20 g mixed bed resin system, a preliminary upscale of the oxidative process was attempted on about 100 g of mixed resin beads loaded with stable isotopes of Cs, Co, Sr, Ni, Cl and I, chosen as representatives of fission and activation products and of the different chemism of nuclides in the process. The increased mass of the mixed bed resin system (above 100 g) involved the introduction of an external heat source to safely initiate the oxidative process. Indeed, a start-up temperature of at least 45 °C ensured by a thermal bath was optimized before adding the oxidant to avoid the unsafe accumulation of unreacted H_2O_2 caused by greater system inertia. The process upscale implemented by this limited experimental setup demanded higher duration from 3 h (20 g) till 8 h (100 g) and 15 h (200 g) at increasing waste mass. However, these time scale factors are to be considered preliminary, since a well-tuned up-scaling in a fitting setup needs to be performed.

As shown in Fig. 4, the upscale made the double-peak oxidative reaction more evident. The first peak (at about 90 °C) is related to the degradation of cationic resin, while a second peak at about 95 °C is representative of the very long decomposition of anionic resin in accordance with literature and first experimental findings (Feng et al., 2018). Furthermore, temperature monitoring of the process off-gases resulted in a profile consistent with that of the solution. Fig. 5 shows the transition from cationic to anionic resin oxidation. At that point, the reaction temperature increased up to about 95 °C, and intense foam generation occurs. This phenomenon became more pronounced when a 200 g mixed resin bed system was treated. In particular, the large presence of foam can lift the resin beads up and hinder the close contact with the oxidant, thereby reducing the effectiveness of the process and increasing its duration. Since foaming is caused by the decomposition of the anionic resin, considerations must be done when changing mass ratios of cationic-to-anionic resins.

At the end of the oxidation, a mixture was obtained constituted of a liquid effluent and a whitish suspension free of resin beads that was left to sediment overnight. Then, an aliquot of the clear solution was taken to monitor the nuclides distribution throughout the process. Notably, more than 99 wt.% of the initial Co, Ni and Cs was found in the resulting solution, while Sr was distributed between the solution (30 wt.%) and precipitate (70 wt.%). As also reported in previous works on cationic resin batches, iron and strontium sulphates were identified in the fine and whitish precipitate at the bottom of the reactor via XRD analysis (Galluccio et al., 2021). On the other hand, only a small amount (approximately 10 wt.%) of I and Cl remains in the final solution according to preliminary analysis. These elements came out as process off-gases and were collected downstream of the glass reactor, as mentioned in the experimental setup section.

As previously described, the mixtures were evaporated at the end of the wet oxidation treatments, and a sludgy residue was obtained. Regardless of the process scale, consistent WRR values of about 75–80 wt.% were found, as proof of the promising process upscale conducted so far. Furthermore, the XRD analyses proved that the Fenton residues are partially crystalline. The diffraction patterns in Fig. 6 show Bragg peaks related to the following inorganic species: dominant ammonium copper sulphate hydrate $(NH_4)_2Cu(SO_4)_2 \cdot 6\ H_2O$ (database ref. code #01-072-1658), chalcanthite $CuSO_4 \cdot 5\ H_2O$ (ref. code #00-011-0646), iron sulphate $FeSO_4$ (ref. code #00-033-0682), and subordinate bonattite $CuSO_4 \cdot 6\ H_2O$ (ref. code #00-012-0262), sabietite $NH_4Fe(SO_4)_2$ (ref. code #00-024-0044), and sal ammoniac NH_4Cl (ref. code #00-002-0887). The residual organic content generates the anomalous background of the diffraction patterns, typical of an amorphous component which is ascribable to residual small organic species.

Thereby, the process scalability and effectiveness in decomposing up to 200 g of mixed bed ion exchange resins were verified, even more with a surrogate waste containing representative contaminants. A higher amount of oxidant and a longer duration of the process were needed, if compared to a cationic resin bed system as shown in Fig. 7 (Galluccio et al., 2024).

3.2. Conditioning in the matrix

Downstream of the evaporation process, the resulting brownish residue has a pH around 0.5, coherently with the fact that it was obtained by concentrating the mineralized aqueous mixture, having pH around 2. Because of this, encapsulation in the alkali-activated matrix previously developed required acidity adjustments (Santi et al., 2022). This allowed to successfully achieve hardening of the formulations loaded up to 40 wt.% of residue.

From a visual inspection of the synthesized specimens, the grouts resulted workable and easily pourable. Furthermore, it was observed that, by increasing the LF, the viscosity of the grout was reduced. Hence, the already adequate workability of the fresh, unloaded matrix,

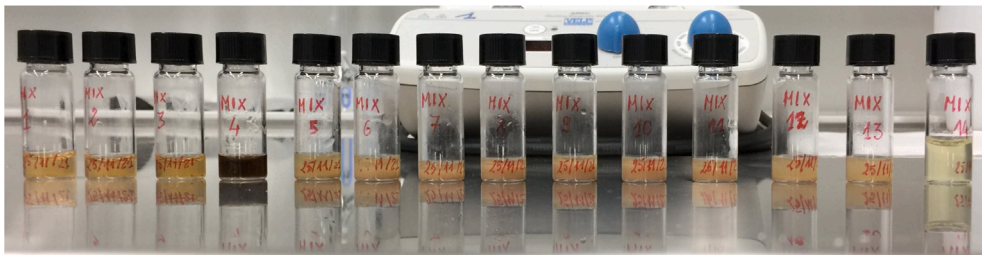

Fig. 3. Aliquots of the wet oxidation mixture periodically collected to monitor the evolution of the oxidative process.

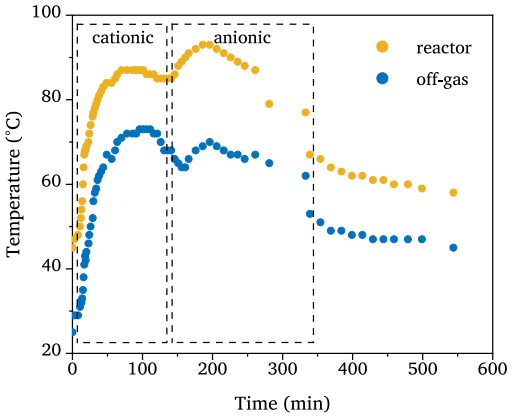

Fig. 4. Reaction temperature profile over time of the mixture and off-gases for the upscale process.

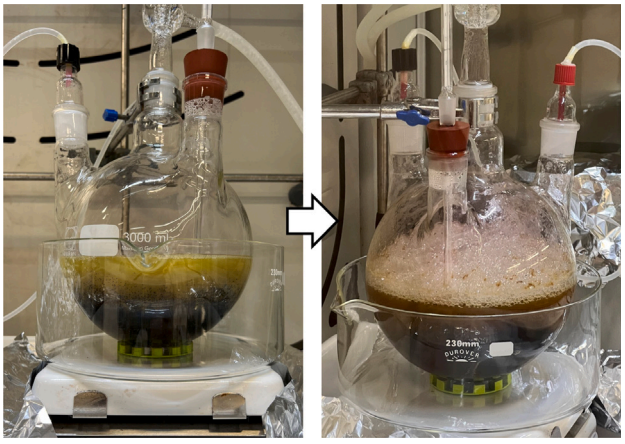

Fig. 5. Transition from cationic (left) to anionic (right) resin oxidation.

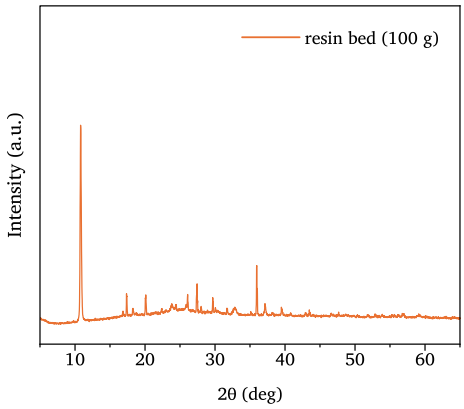

Fig. 6. X-ray diffraction patterns of the final residues obtained from the intermediate laboratory scale (100 g) process. The Bragg peaks related to the following inorganic species have been assigned as reported in the text.

measured in a previous work (Santi et al., 2022), further improves by increasing the wet oxidation residue content. This is evident also in cubic samples cast for compression tests, some of which are reported in Fig. 8: cavities decrease in number and size with increasing LF, resulting in increased homogeneity.

The XRD patterns of the matrix and of the waste forms are reported in Fig. 9. The pattern of the matrix (0 wt.% LF) confirms the results previously found, with a pronounced background generated by the amorphous component of the mix and related to the activation and reaction of the powdery precursors (Costa et al., 2021), while the diffraction peaks are associated to the following crystalline species: dominant quartz SiO_2 (database ref. code #01-088-2487) and zeolite chabazite $|(Ca_{0.5},K,Na)_x(H_2O)_{12}|[Al_xSi_{12-x}O_{24}]$, with x within 2.4 - 5.0 (ref. code #01-086-2115), subordinate zeolite phillipsite $|(Ca_{0.5},Na,K)_x(H_2O)_{12}|[Al_xSi_{16-x}O_{32}]$, with x within 4.1 - 6.8 (ref. code #00-034-0542), and probable hydrotalcite $(Mg_6Al_2CO_3(OH)_{16} \cdot 4\ H_2O)$ (ref. code #00-041-1428). The diffraction pattern of the loaded waste form exhibits increased amorphousness due to the organic residue within the loaded waste (Fig. 9). Additional peaks related to thenardite Na_2SO_4 (ref. code #01-074-2036) and other sulphates, such as chalcanthite $CuSO_4 \cdot 5\ H_2O$ (ref. code #00-011-0646) and gypsum $CaSO_4 \cdot 2\ H_2O$ (ref. code #01-076-1746) are found. The newly formed species (Na_2SO_4 and $CaSO_4$) are likely generated from the interaction of the residue, which contains sulphates and sulphuric acid, with the NaOH (used in the neutralization and alkali-activation steps) and the BFS (used as precursor of the conditioning matrix). The presence of chabazite in the pristine tuff and in the final waste forms should guarantee enhanced retention of Cs, which is a highly mobile species. Indeed, chabazite is known for its high affinity towards Cs (Cappelletti et al., 2011; Baek et al., 2018; Kwon et al., 2021).

3.3. Qualification of waste forms

Hardened matrices and waste forms underwent preliminary immersion in de-ionized water for two weeks. All samples loaded with waste coloured the water within a few hours because of the release of chemical species. The sample loaded at 10 wt.% with the Fenton residue had slight surface cracks, mainly attributable to post-immersion drying. No fragments were found at the bottom of the immersion jar for this sample. The situation was different for the 20 wt.% loaded specimens, where the number of fragments at the bottom of the jar was significant. In addition, these specimens exhibited fractures during immersion due to swelling, probably as a result of moisture intake. Thus, the presence of fragments at the bottom of the jars can be attributed to the dimensional instability of the waste forms. The situation is intensified for samples loaded up to 40 wt.%, for which the volumetric instabilities are greater, and the specimens fail the immersion test, fragmenting into several pieces found at the bottom of the jars. For these reasons, specimens with LF above 20 wt.% were discarded.

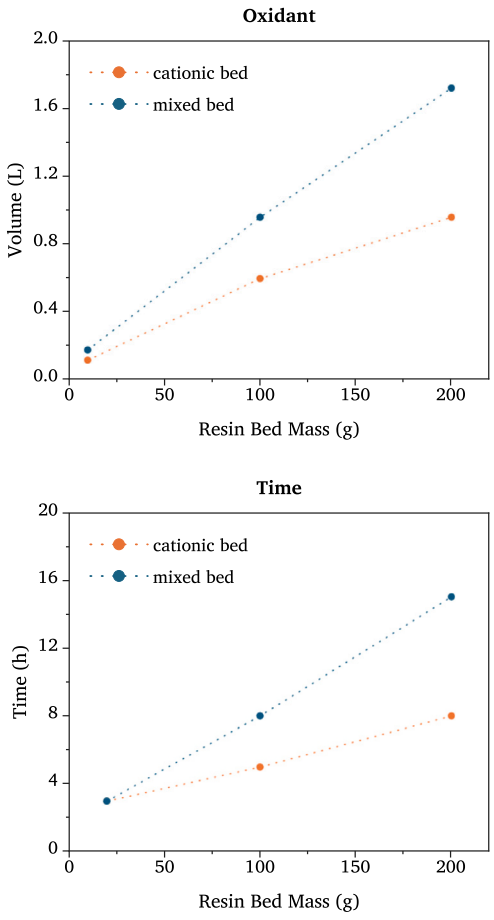

Fig. 7. Comparison of the oxidant amount (top) and process duration (bottom) between the cationic and mixed bed resin systems at increasing surrogate waste mass.

The compression tests were carried out on cubic samples with side 5 cm, with wet oxidation residues loaded up to 20 wt.%. The results are reported in Fig. 10. The compressive strength of waste forms decreases with increasing LF. Given the little interaction of the waste with the matrix suggested by microstructural analysis, this deterioration is attributed to the decrease in the resistant section of the matrix within the specimens, which is replaced by the waste. Compressive strengths for 20 wt.% loaded specimens are greater than the reference value of 10 MPa, thereby satisfying the acceptance criterion (Ispettorato nazionale per la sicurezza nucleare e la radioprotezione, 2022). In regard to the LF, it is evident that any increase beyond 20 wt.% would bring the compressive strength of the waste forms below the minimum Italian requirements (Fig. 10). Hardening of waste forms was demonstrated up to 40 wt.%, thus fostering efforts to improve the matrix formulation to allow higher loading factors. Nevertheless, higher loading factors could already satisfy less stringent requirements from other countries.

Specimens loaded at 10 wt.% and 20 wt.% with Fenton residues underwent leaching test according to the ANSI/ANS-16.1-2019 protocol (American National Standards Institute, 2019), as per Italian WAC (Ispettorato nazionale per la sicurezza nucleare e la radioprotezione, 2022). After one day of immersion, samples loaded at 20 wt.% fragmented and partially dissolved, as evidenced by the intense coloration of the leachate and the releases estimated by ICP-MS and ICP-OES, which resulted to be from one to two orders of magnitude greater than those of samples loaded at 10 wt.% at 7 days. In contrast, the samples loaded at 10 wt.% withstood one week of immersion. Fig. 11 shows the cumulative releases of some matrix constituents, such as Na, Si, and Al, and some waste contaminants such as S, Cs, and Cl. The leachability indices of the investigated species are reported in Fig. 12. Although the protocol used for leaching is limited in providing information on the mechanism of the release of chemical species, the linearity of cumulative releases as a function of the square root of time suggests a predominantly diffusive mechanism (Hinsenveld, 1991; Abdel Rahman et al., 2007).

Table 4
Results of mercury intrusion porosimetry.

Specimen	Average pore diameter (nm)	Porosity (%)
10 wt.% waste loading, non-immersed	32.8	41.6
10 wt.% waste loading, immersed	39.8	53.2
20 wt.% waste loading, non-immersed	33.5	48.4

The lowest releases, and thus the highest indices, are associated with Si, Al and Ca, which are bound within the matrix. In contrast, the highest releases, and thus the lowest indices, are those of Na, because it is unbound in the matrix and easily leached given the small size of the Na^+ cation. It is also observed that Cl has releases compatible in magnitude with Na, suggesting that it does not form compounds and, therefore is easily leachable. Conversely, Cs and Sr are well retained in the waste form. From the diffraction patterns of the matrix and the waste forms (Fig. 9), the distinctive chabazite and phillipsite peaks are observed. Regarding this, literature works on the selectivity of these zeolites towards Cs and Sr are numerous. Baek et al. (2018) reported high Cs selectivity for chabazite. On the other side, Sr could as well precipitate as $SrSO_4$ in small amounts, which were not detected by XRD. Therefore, it is reasonable to think that these two cations interact within the matrix. Other metal contaminants, such as Co and Ni, also exhibit very low releases. This is due to their precipitation as hydroxides in the highly alkaline environment of the matrix, which are known to be stable and insoluble even at other pH (Fu et al., 2011). Given the low concentrations of Co and Ni in the matrix, an absence of $Co(OH)_2$ and $Ni(OH)_2$ diffraction peaks in the XRD patterns is expected. A different situation is that of S, which is leached in large quantities. XRD analyses identify the presence of many sulphates in the waste forms, the main one being Na_2SO_4, in the form of thenardite. Sodium sulphate is insoluble at high pH, it precipitates during waste basification and remains so during mixing of fresh grouts. Indeed, no peaks of thenardite are observed in the XRD patterns of the acidic Fenton residues (Fig. 9). When the specimen is subsequently immersed, the contact with ultrapure water at lower pH promotes the dissolution of Na^+ and SO_4^{2-}. This explains the particularly low leaching indices of Na and S and the absence of thenardite in the XRD diffractograms of the specimens after water immersion, which is the most appreciable difference between the pattern reported in Fig. 13.

The pore microstructure of the specimens loaded at 10 wt.% and 20 wt.% with the Fenton residues is instead reported in Table 4 and Fig. 14. The coarseness of the samples increases as the waste LF increases and as a result of immersion. In all cases, most pores have diameters between 2 and 100 nm, and between 10 and 150 μm. Increasing the LF to 20 wt.% increases the porosity to 48%, which is compatible with the observed decrease of the compressive strength (Fig. 10). The increase in porosity is probably due to a foaming effect of the residual small organic species present in the Fenton residue, which occurs during the preparation of fresh grouts. This high porosity explains the leaching behaviour: due to increased porosity, the permeability increases, along with the diffusion coefficients of various chemical species. In addition, swelling is more intense as the volume exposed to water increases and, therefore, internal stress within the material causes the specimen to fragment, resulting in exposure of a larger surface area to the leachant and higher releases. During water immersion, there is also a phenomenon of dissolution of some species, including Na_2SO_4 identified by XRD (Fig. 13), which were previously precipitated and, therefore, new pores are generated as a consequence. The newly generated pores thus are more likely to be interconnected and, in fact, the average diameter increases by about 20% (Table 4).

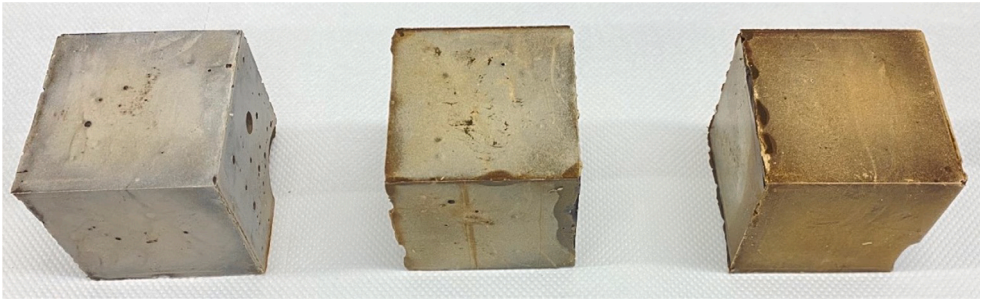

Fig. 8. Hardened cubic specimens for compressive strength. From left to right: 0, 10, and 20 wt.% loading factors.

Table 5
Literature overview about encapsulation of spent resins in alkaline matrices.

Reference	WRR (wt.%)	LF (wt.%)	effective conditioning factor (ECF) (kg kg^{-1})	Resin bed	Matrix
This work	80	10	0.57	Mixed	Tuff-based alkali-activated matrix
De Araujo et al. (2018)	90	22	2.82	Mixed	Sulfoaluminate cement
Xu et al. (2022)		40	0.67	Cationic	Sulfoaluminate cement
Lin et al. (2020)		12	0.14	Cationic	Metakaolin- and slag-based geopolymer
Pan et al. (2001)		30	0.43	Mixed	Portland cement I
Bagosi et al. (1999)		17	0.20	Cationic	Ordinary Portland cement
Lee et al. (2019)		32	0.47	Mixed	Slag-based geopolymer
Junfeng et al. (2005)		40	0.67	Mixed	Activated slag cement

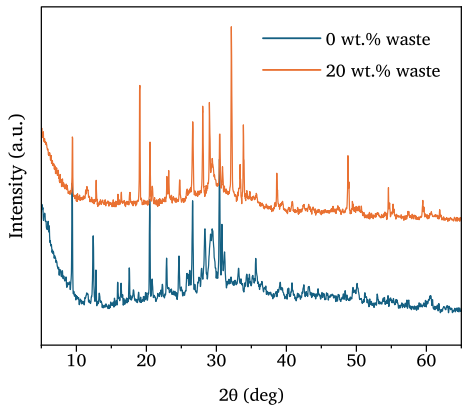

Fig. 9. X-ray diffraction pattern of the hardened matrix (0 wt.% LF) and waste forms (20 wt.% LF). The Bragg peaks related to the following inorganic species have been assigned as reported in the text.

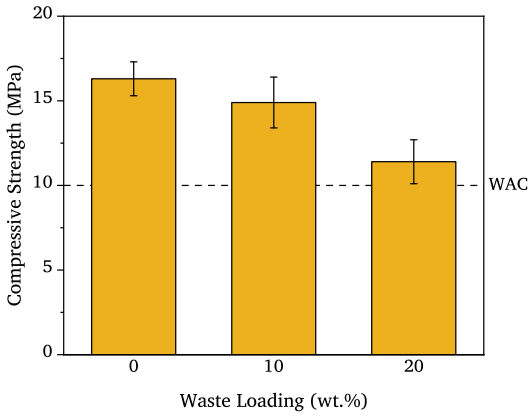

Fig. 10. Compressive strength of cubic specimens loaded with sludgy waste downstream of treatment process. The dotted represents the Italian acceptance criterion (Ispettorato nazionale per la sicurezza nucleare e la radioprotezione, 2022), taken as reference.

3.4. *Effectiveness of the strategy*

It is worth comparing the proposed management strategy with the recent existing literature. Some literature works are reported in Table 5. The WRR and LF are computed as in Eqs. (1) and (2), respectively. To consider the effectiveness of the overall management strategy (treatment and conditioning) to reduce volumes of final waste forms, the ECF is calculated as reported in Eq. (3) considering the mass of the resin (m_{res}) and the mass of the matrix (m_m):

$$\mathrm{ECF} = \frac{m_{res}}{m_m}. \tag{3}$$

Consequently, the higher the value of ECF, the lower the mass (and volume) increment of the final waste forms. Eq. (3) can be written in a more practical form, as reported in Eq. (4), by taking advantage of Eqs. (1) and (2):

$$\mathrm{ECF} = \frac{\mathrm{LF}}{1-\mathrm{LF}} \times \frac{1}{1-\mathrm{WRR}}. \tag{4}$$

This allows to easily convert and compare results of this work with those from the literature. In case no treatment is carried out, WRR is taken to be null and the ECF only depends on the LF. As reported in Table 5, whatever the conditioning matrix, the combination of treatment and immobilization almost results in higher resin encapsulation factors. In contrast, the direct conditioning option results in lower encapsulation factors, due to limitations in matrices loading capacity caused by the low compatibility with organic matter and by deterioration of the long-term durability of the waste forms. Even though both the treatment and the conditioning processes investigated in this work are at a preliminary laboratory level of development, the overall mass (or volume) optimization achieves higher values, at the expense of increased complexity of the management strategy. A noteworthy advantage of the preliminary treatment is the decomposition of organic matter, with undisputed improvement of disposability due to limitations in organic material capacity of repositories and better long-term durability of the final waste forms. Hence, this integrated approach has shown some promises and deserves future study aimed at optimizing both WRR and LF factors, considering sustainability aspects and ease of application.

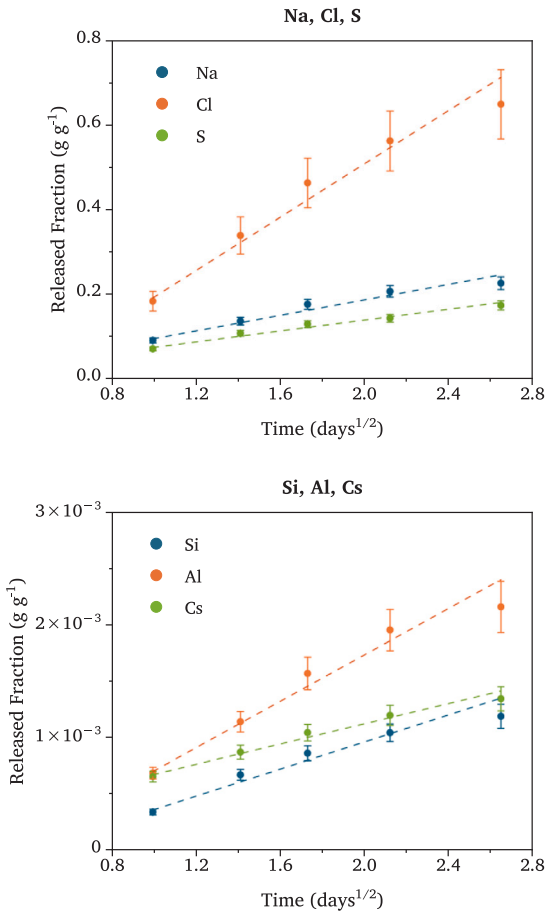

Fig. 11. Cumulative releases of Na, Cl, and S (top) and of Si, Al, and Cs (bottom) for the specimens loaded at 10 wt.% with the Fenton residue.

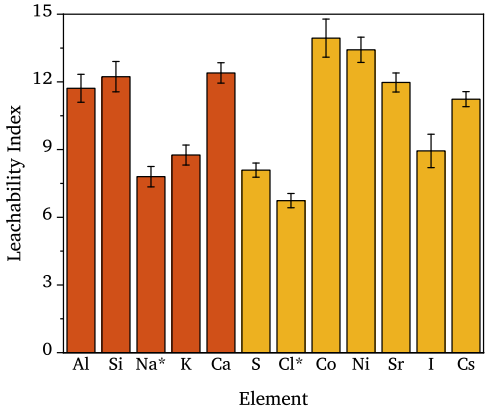

Fig. 12. Leachability indices for both matrix constituents (Si, Al, Ca, K), in orange, and waste contaminants (S, Co, Ni, Sr, Cs, Cl, I), in yellow, for the specimens loaded at 10 wt.% with the Fenton residues. The asterisk refers to elements for which the hypothesis of the leaching protocol is less appropriate.

4. Conclusion

To the best of the authors' knowledge, for the first time, the Fenton wet oxidation residues were successfully encapsulated in a non-cementitious matrix, revealing a promising and sustainable integrated pre-disposal management of spent IERs. Indeed, the combination of low temperatures, green oxidant, natural, low-cost materials and recycled industrial by-products as matrix precursors are key points towards a

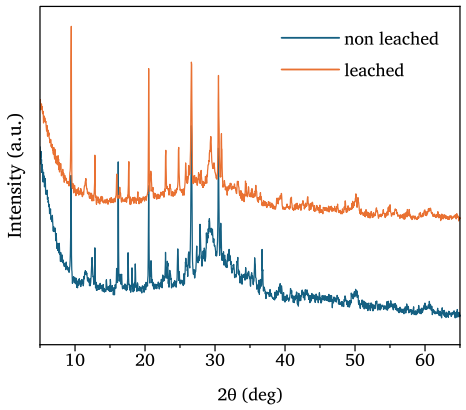

Fig. 13. Diffraction patterns of specimens loaded at 10 wt.% before and after leaching. The Bragg peaks related to the following inorganic species have been assigned as reported in the text.

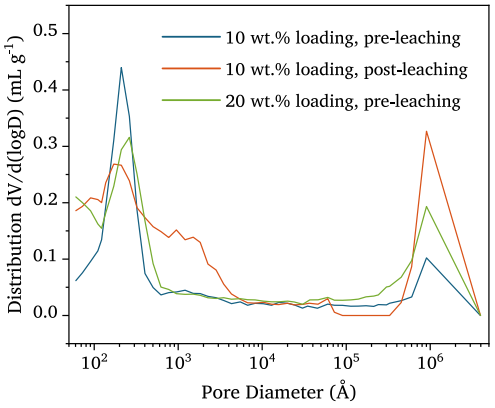

Fig. 14. Pore size distributions in specimens loaded with Fenton residues.

sustainable disposal strategy. The preliminary results obtained in this work demonstrate the feasibility, scalability, and effectiveness of spent IERs treatment by Fenton wet oxidation process. The tests performed on surrogate IERs showed promising WRR. Promising correlations were found among different batch sizes, suggesting the feasibility of the upscale of the oxidizing process. Moreover, aware of the benefits of this technology for the future of nuclear industry in the treatment of problematic organic radioactive waste, a larger upscale of the process can be attempted thus demonstrating the same efficacy for the management of about 1 kg of spent mixed bed IERs.

Regarding the encapsulation of the treated residue, the use of additional NaOH for wet oxidation residues neutralization allowed to successfully achieve hardening of the fresh grouts. A residue immobilization up to 40 wt.% was obtained, and compressive strength of hardened waste forms was proved to be compliant with Italian WAC up to 20 wt.% LF. Such a condition corresponds to a greater mass of spent resin with respect to the mass of the matrix used for its immobilization, thus allowing an overall optimization in terms of masses (and volumes) of the management strategy. The preliminary compressive strength and leaching data corroborate the promising stability of the waste form and promote further investigations to fully demonstrate the compliance with WAC. Physical and chemical stability of the hardened forms, as well as their durability and process parameters (*e.g.*, workability, setting time, optimal curing conditions) will be addressed to further optimize the process before implementing this technology at an industrial scale.

Funding sources

The EU H2020 PREDIS project has received funding from the Euratom research and training program 2019–2020 under grant agreement No 945098.

Abbreviations

BFS	Blast-furnace slag
COD	Chemical oxygen demand
ECF	Effective conditioning factor
FA	Fly ash
IER	Ion-exchange resin
ICP-MS	Inductively coupled plasma mass spectrometry
ICP-OES	Inductively coupled plasma optical emission spectroscopy
LF	Loading factor
VT	Volcanic tuff
WAC	Waste acceptance criteria
WRR	Weight reduction ratio
XRD	X-ray powder diffraction
XRF	X-ray fluorescence

CRediT authorship contribution statement

Francesco Galluccio: Writing – original draft, Methodology, Investigation, Data curation, Conceptualization. **Andrea Santi:** Writing – original draft, Methodology, Investigation, Data curation, Conceptualization. **Eros Mossini:** Writing – review & editing, Project administration, Funding acquisition, Conceptualization. **Gabriele Magugliani:** Writing – review & editing, Methodology, Conceptualization. **Fabio Fattori:** Writing – review & editing, Methodology. **Giacomo Diego Gatta:** Writing – review & editing, Investigation. **Paolo Lotti:** Writing – review & editing, Investigation. **Davide Cori:** Writing – review & editing, Investigation. **Elena Macerata:** Writing – review & editing. **Gianmarco Bilancia:** Supervision, Resources. **Mario Mariani:** Supervision, Resources.

Declaration of competing interest

The authors declare that they have no known competing financial interests or personal relationships that could have appeared to influence the work reported in this paper.

Data availability

No data was used for the research described in the article.

Acknowledgements

F. Galluccio acknowledges the Collaborative Doctoral Partnership between Politecnico di Milano and European Commission's Joint Research Centre – Ispra site. Besides, special thanks go to Idreco S.r.l. company for providing Amberlite™ IRN 77–78 ion exchange resins, and to Buzzi Unicem S.p.A. and Fertenia S.r.l. companies for providing encapsulation materials. The authors acknowledge Roberto Losi from the Laboratory of Catalysis and Catalytic Processes of Politecnico di Milano for performing Mercury Intrusion Porosimetry analysis.

References

Abdel Rahman, R.O., et al., 2007. Modeling the long-term leaching behavior of ^{137}Cs, ^{60}Co, and ^{152,154}Eu radionuclides from cement–clay matrices. J. Hazard. Mater. 145, 372–380. http://dx.doi.org/10.1016/j.jhazmat.2006.11.030.

Ahmed, M.M., et al., 2021. Fabrication of thermal insulation geopolymer bricks using ferrosilicon slag and alumina waste. Case Stud. Constr. Mater. 15, 1–14. http://dx.doi.org/10.1016/j.cscm.2021.e00737.

American National Standards Institute, 2019. Measurement of the leachability of solidified of low-level radioactive wastes by a short-term test procedure. ANSI/ANS-16.1-2019.

Autef, A., et al., 2013. Role of the silica source on the geopolymerization rate: A thermal analysis study. J. Non-Cryst. Solids 366, 13–21. http://dx.doi.org/10.1016/j.jnoncrysol.2013.01.034.

Baek, W., et al., 2018. Cation exchange of cesium and cation selectivity of natural zeolites: Chabazite, stilbite, and heulandite. Microporous Mesoporous Mater. 264, 159–166. http://dx.doi.org/10.1016/j.micromeso.2018.01.025.

Bagosi, S., et al., 1999. Immobilization of caesium-loaded ion exchange resins in zeolite-cement blends. Cem. Concr. Res. 29, 479–485. http://dx.doi.org/10.1016/S0008-8846(98)00190-2.

Bokare, A.D., et al., 2014. Review of iron-free Fenton-like systems for activating H_2O_2 in advanced oxidation processes. J. Hazard. Mater. 275, 121–135. http://dx.doi.org/10.1016/j.jhazmat.2014.04.054.

Cappelletti, P., et al., 2011. Immobilization of Cs and Sr in aluminosilicate matrices derived from natural zeolites. J. Nucl. Mater. 414, 451–457. http://dx.doi.org/10.1016/j.jnucmat.2011.05.032.

Castro, H.A., et al., 2018. Study of plasma off-gas treatment from spent ion exchange resin pyrolysis. Environ. Sci. Pollut. Res. 25, 21403–21410. http://dx.doi.org/10.1007/s11356-017-8766-2.

Costa, L.M., et al., 2021. Influence of the addition of amorphous and crystalline silica on the structural properties of metakaolin-based geopolymers. Appl. Clay Sci. 215, 1–13. http://dx.doi.org/10.1016/j.clay.2021.106312.

De Araujo, L.G., et al., 2018. Reaction of ion exchange resins with Fenton's reagent. Environments 5, 1–10. http://dx.doi.org/10.3390/environments5110123.

de Azevedo, A.R.G., et al., 2017. Influence of incorporation of glass waste on the rheological properties of adhesive mortar. Constr. Build. Mater. 148, 359–368. http://dx.doi.org/10.1016/j.conbuildmat.2017.04.208.

de Oliveira, L.B., et al., 2022. Durability of geopolymers with industrial waste. Case Stud. Constr. Mater. 16, 1–25. http://dx.doi.org/10.1016/j.cscm.2021.e00839.

Desotelle, G., 1999. METHOD 14XXXCOD: Chemical oxygen demand (COD) by dichromate oxidation and photometry.

2023a. AmberLite™ IRN77 H ion exchange resin: Nuclear-grade, uniform particle size, gel, strong base cation exchange resin for water treatment applications in the nuclear power industry. DuPont™.

2023b. AmberLite™ IRN78 OH ion exchange resin: Nuclear-grade, uniform particle size, gel, strong base anion exchange resin for water treatment applications in the nuclear power industry. DuPont™.

Dyer, A., et al., 2000. The use of natural zeolites for radioactive waste treatment: Studies on leaching from zeolite/cement composites. J. Radioanal. Nucl. Chem. 243, 839–841. http://dx.doi.org/10.1023/A:1010632000600.

European Committee for Standardization, 2019. Testing hardened concrete - Part 3: Compressive strength of test specimens. EN 12390-3.

European Committee for Standardization, 2021. Testing hardened concrete - Part 1: Shape, dimensions and other requirements for specimens and moulds. EN 12390-1.

Feng, W., et al., 2018. The treatment of IRN77/78 resin using Fenton oxidation process. IOP Conf. Ser.: Mater. Sci. Eng. 392, 1–7. http://dx.doi.org/10.1088/1757-899X/392/3/032042.

Firdous, R., et al., 2018. Natural pozzolan based geopolymers: A review on mechanical, microstructural and durability characteristics. Constr. Build. Mater. 190, 1251–1263. http://dx.doi.org/10.1016/j.conbuildmat.2018.09.191.

Fu, F., et al., 2011. Removal of heavy metal ions from wastewaters: A review. J. Environ. Manag. 92, 407–418. http://dx.doi.org/10.1016/j.jenvman.2010.11.011.

Gallé, C., 2001. Effect of drying on cement-based materials pore structure as identified by mercury intrusion porosimetry: A comparative study between oven-, vacuum-, and freeze-drying. Cem. Concr. Res. 31, 1467–1477. http://dx.doi.org/10.1016/S0008-8846(01)00594-4.

Galluccio, F., et al., 2021. Promising pre-disposal solutions to manage spent radioactive ion-exchange resins. In: International Conference on Radioactive Waste Management: Solutions for a Sustainable Future. Vol. 1, p. 127.

Galluccio, F., et al., 2024. Innovative oxidative treatment and geopolymer encapsulation of spent mixed bed ion exchange resins. In: Book of Abstracts of the 10th European Commission Conferences on EURATOM Research and Training in Safety of Reactor Systems & Radioactive Waste Management. Vol. 2, pp. 351–353.

Görhan, G., et al., 2014. The influence of the NaOH solution on the properties of the fly ash-based geopolymer mortar cured at different temperatures. Composites B 58, 371–377. http://dx.doi.org/10.1016/j.compositesb.2013.10.082.

Hafeez, M.A., et al., 2021. Fenton-like treatment for reduction of simulated carbon-14 spent resin. J. Environ. Chem. Eng. 9, 9. http://dx.doi.org/10.1016/j.jece.2020.104740.

Hinsenveld, M., 1991. Towards a new approach in modeling leaching behavior. Stud. Environ. Sci. 48, 331–340. http://dx.doi.org/10.1016/S0166-1116(08)70417-5.

Huang, C., et al., 2020. Oxidative dissolution of cation ion exchange resin by the Fenton process using a fluidized bed reactor. Prog. Nucl. Energy 125, 1–8. http://dx.doi.org/10.1016/j.pnucene.2020.103377.

International Atomic Energy Agency, 1993. Treatment and conditioning of spent ion exchange resins from research reactors, precipitation sludges and other radioactive concentrates. In: Technical Documents Series, vol. 689, pp. 1–62.

International Atomic Energy Agency, 2001. Handling and processing of radioactive waste from nuclear applications. In: Technical Reports Series, vol. 402, pp. 1–141.

International Atomic Energy Agency, 2017. Selection of technical solutions for the management of radioactive waste. In: Technical Documents Series, vol. 1817, pp. 1–95.

International Standardisation Organisation, 2022. Water quality - Determination of the chemical oxygen demand index (ST-COD) - Small-scale sealed-tube method.

Ispettorato nazionale per la sicurezza nucleare e la radioprotezione, 2022. Technical guide 33 - Safety criteria for radioactive waste management. (document written in Italian).

Junfeng, L., et al., 2005. Solidification of low-level-radioactive resins in ASC-zeolite blends. Nucl. Eng. Des. 235, 817–820. http://dx.doi.org/10.1016/j.nucengdes.2004.10.008.

Khalifeh, M., et al., 2014. Potential utilization of class C fly ash-based geopolymer in oil well cementing operations. Cem. Concr. Compos. 53, 10–17. http://dx.doi.org/10.1016/j.cemconcomp.2014.06.014.

Kwon, S., et al., 2021. Relationship between zeolite structure and capture capability for radioactive cesium and strontium. J. Hazard. Mater. 408, 1–9. http://dx.doi.org/10.1016/j.jhazmat.2020.124419.

Lama, G., et al., 2022. Heterogeneous advanced oxidation processes: Current approaches for wastewater treatment. Catalysts 12, 1–31. http://dx.doi.org/10.3390/catal12030344.

Lee, W., et al., 2019. Geopolymer technology for the solidification of simulated ion exchange resins with radionuclides. J. Environ. Manag. 235, 19–27. http://dx.doi.org/10.1016/j.jenvman.2019.01.027.

Lin, W., et al., 2020. Performance study of ion exchange resins solidification using metakaolin-based geopolymer binder. Prog. Nucl. Energy 129, 1–7. http://dx.doi.org/10.1016/j.pnucene.2020.103508.

Liou, R., et al., 2005. Fe (III) supported on resin as effective catalyst for the heterogeneous oxidation of phenol in aqueous solution. Chemosphere 59, 117–125. http://dx.doi.org/10.1016/j.chemosphere.2004.09.080.

Meng, X., et al., 2022. Degradation of the mixed nuclear-grade cationic and anionic exchange resins using Fe^{2+}/H^{+} homogeneous Fenton oxidation. Environ. Res. 212, 1–14. http://dx.doi.org/10.1016/j.envres.2022.113400.

Office of Federal, et al., 2013. Final Comparative Environmental Evaluation of Alternatives for Handling Low-Level Radioactive Waste Spent Ion Exchange Resins from Commercial Nuclear Power Plants. U.S. Nuclear Regulatory Commission, pp. 1–208.

Oksa, M., et al., 2021. Proceedings of PREDIS may workshop 2021. pp. 1–106, PREDIS Project.

Pan, L.K., et al., 2001. Optimization for solidification of low-level-radioactive resin using Taguchi analysis. Waste Manage. 21, 767–772. http://dx.doi.org/10.1016/S0956-053X(01)00012-5.

Pan, Z., et al., 2009. An investigation of the mechanisms for strength gain or loss of geopolymer mortar after exposure to elevated temperature. J. Mater. Sci. 44, 1873–1880. http://dx.doi.org/10.1007/s10853-009-3243-z.

Perez-Cortes, P., et al., 2024. Cementation of spent radioactive ion-exchange resin ashes using alkali-activated cements: Physicochemical and structural changes. Cem. Concr. Compos. 149, 1–15. http://dx.doi.org/10.1016/j.cemconcomp.2024.105517.

Reeb, C., et al., 2021. Incorporation of organic liquids into geopolymer materials - A review of processing, properties and applications. Ceram. Int. 47, 7369–7385. http://dx.doi.org/10.1016/j.ceramint.2020.11.239.

Rozek, P., et al., 2019. Geopolymer-zeolite composites: A review. J. Clean. Prod. 230, 557–579. http://dx.doi.org/10.1016/j.jclepro.2019.05.152.

Santi, A., et al., 2022. Design of sustainable geopolymeric matrices for encapsulation of treated radioactive solid organic waste. Front. Mater. 9, 1–17. http://dx.doi.org/10.3389/fmats.2022.1005864.

Singh, B., et al., 2015. Geopolymer concrete: A review of some recent developments. Constr. Build. Mater. 85, 78–90. http://dx.doi.org/10.1016/j.conbuildmat.2015.03.036.

Taylor, H.F.W., et al., 2001. Delayed ettringite formation. Cem. Concr. Res. 31, 683–693. http://dx.doi.org/10.1016/S0008-8846(01)00466-5.

Vilve, M., et al., 2010. Degradation of 1,2-dichloroethane from wash water of ion-exchange resin using Fenton's oxidation. Environ. Sci. Pollut. Res. 17, 875–884. http://dx.doi.org/10.1007/s11356-009-0291-5.

Walling, S.A., et al., 2021. Fenton and Fenton-like wet oxidation for degradation and destruction of organic radioactive wastes. Npj Mater. Degradation 5, 1–20. http://dx.doi.org/10.1038/s41529-021-00192-3.

Wan, Z., et al., 2015. Disintegration and dissolution of spent radioactive cationic exchange resins using Fenton-like oxidation process. Nucl. Eng. Des. 291, 101–108. http://dx.doi.org/10.1016/j.nucengdes.2015.05.009.

Wan, Z., et al., 2016. Treatment of spent radioactive anionic exchange resins using Fenton-like oxidation process. Chem. Eng. J. 248, 733–740. http://dx.doi.org/10.1016/j.cej.2015.09.004.

Wang, J., et al., 2015. Treatment and disposal of spent radioactive ion-exchange resins produced in the nuclear industry. Prog. Nucl. Energy 78, 47–55. http://dx.doi.org/10.1016/j.pnucene.2014.08.003.

Wang, N., et al., 2016. A review on Fenton-like processes for organic wastewater treatment. J. Environ. Chem. Eng. 4, 762–787. http://dx.doi.org/10.1016/j.jece.2015.12.016.

Xu, L., et al., 2019. Dissolution and degradation of nuclear grade cationic exchange resin by Fenton oxidation combining experimental results and DFT calculations. Chem. Eng. J. 361, 1511–1523. http://dx.doi.org/10.1016/j.cej.2018.09.169.

Xu, J., et al., 2022. Metakaolin-reinforced sulfoaluminate-cement-solidified wasteforms of spent radioactive Resins—optimization by a mixture design. Coatings 12, 1–12. http://dx.doi.org/10.3390/coatings12101466.

Zahorodna, M., et al., 2007. Application of the Fenton process to the dissolution and mineralization of ion exchange resins. Catal. Today 129, 200–206. http://dx.doi.org/10.1016/j.cattod.2007.08.014.

Zahorodna, M., et al., 2008. Dissolution and mineralization of ion exchange resins: differentiation between heterogeneous and homogeneous (photo-)Fenton processes. Photochem. Photobiol. Sci. 7, 1480–1492. http://dx.doi.org/10.1039/b813866b.